Local Density of States at Metal-Semiconductor Interfaces: An Atomic Scale Study

T. Iffländer,[1] S. Rolf-Pissarczyk,[1] L. Winking,[1] R. G. Ulbrich,[1] A. Al-Zubi,[2] S. Blügel,[2] and M. Wenderoth[1,*]
[1]IV. Physical Institute - Solids and Nanostructures, Georg-August-Universität Göttingen, Friedrich-Hund-Platz 1, 37077 Göttingen, Germany
[2]Peter Grünberg Institut and Institute for Advanced Simulation, Forschungszentrum Jülich and JARA, 52425 Jülich, Germany

(Received 5 November 2014; published 9 April 2015)

We investigate low temperature grown, abrupt, epitaxial, nonintermixed, defect-free *n*-type and *p*-type Fe/GaAs(110) interfaces by cross-sectional scanning tunneling microscopy and spectroscopy with atomic resolution. The probed local density of states shows that a model of the ideal metal-semiconductor interface requires a combination of metal-induced gap states and bond polarization at the interface which is nicely corroborated by density functional calculations. A three-dimensional finite element model of the space charge region yields a precise value for the Schottky barrier height.

DOI: 10.1103/PhysRevLett.114.146804 PACS numbers: 73.20.-r, 68.37.Ef, 73.30.+y

About 75 years ago, Schottky [1] and Mott [2] identified the Schottky barrier (SB) height at metal-semiconductor (MS) interfaces as the difference between the work function of the metal and the electron affinity of the semiconductor in contact. However, subsequent measurements revealed a much weaker dependence of the SB height on the metal work function [3,4]. In the literature this effect is often referred to as "Fermi level pinning" and is explained by introducing an additional interface dipole. The origin of this interface dipole remains controversial up to the present day. Some models attribute the Fermi level pinning to metal-induced gap states (MIGS) [5–8], which are identified as evanescent states of the complex band structure in the semiconductor band gap. Thus, MIGS are described as an intrinsic property of the semiconductor. Other models assume that the metal growth process generates defects at the interface giving rise to states that pin the Fermi level at characteristic energies in the band gap [9]. A third kind of model identifies the interface dipole with the polarization of chemical bonds at the interface [10,11]. In this so-called bond polarization model the charge rearrangement associated with the formation of the chemical bonds depends on the metal as well as on the detailed atomic structure of the interface.

In fact, experimental studies focusing on SB formation of atomically controlled epitaxial interfaces [12–16] clearly demonstrate a dependence of the SB height on the atomic orientation and structure of the ordered MS interface. However, these measurements do not yield any information on the local atomic structure itself. Moreover, ballistic electron emission microscopy (BEEM) measurements [17–19] demonstrate lateral inhomogeneities of the SB height on the nanometer scale. Nevertheless, also BEEM does not allow conclusions on the structural properties of the interface. Furthermore, scanning tunneling microscopy (STM) and spectroscopy (STS) studies were performed on top of metal clusters on GaAs(110) [20–23]. However, due to the planar geometry the STM tip probed the MS interface only indirectly. Reusch *et al.* performed STM/STS measurements of Au/GaAs(110) contacts in cross-sectional geometry [24,25]. Nevertheless, due to sample preparation the Au/GaAs(110) interface was not directly accessible. Therefore, to the best of our knowledge, up until now no experiment has been reported that allows a simultaneous structural and electronic investigation of a MS interface in real space with atomic resolution. However, a "complete" energetic and spatial map of the local density of states (LDOS) covering the band gap region and including valence and conduction bands at the interface is of essential importance to check the validity of any proposed model.

In order to close this gap, in this Letter we present an experimental investigation of an abrupt, epitaxial, nonintermixed, defect-free, i.e., an ideal MS interface. In combination with density functional theory calculations we understand the relevance of MIGS and bond polarization at the interface. As a sample system we choose the Fe/GaAs(110) interface because it exhibits a small lattice mismatch of about 1.4% [26] and allows the growth of abrupt high quality epitaxial interfaces [26,27]. Furthermore, the GaAs(110) surface does not exhibit any intrinsic surface states within the fundamental band gap [28] and, therefore, is excellently suited to investigate interface-induced gap states. To obtain information on the atomic structure at the interface we study the interface with atomically resolved STM in cross-sectional geometry [see Fig. 1]. By applying atomically resolved cross-sectional STS covering the energy range of the band gap and a substantial part of the valence and conduction band we explore the LDOS at the interface and the process of SB formation on the atomic scale.

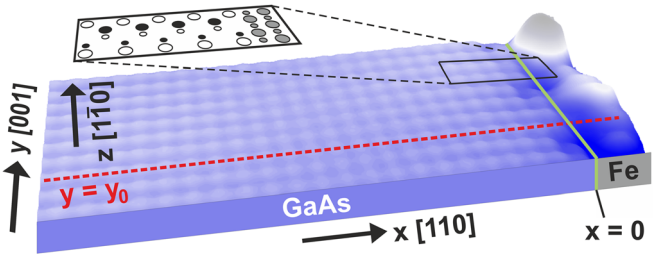

FIG. 1 (color online). 10×5 nm^2 constant current topography of an ideal Fe/n-GaAs(110) interface ($V_s = 2$ V, $I_T = 100$ pA) and cross-sectional geometry. The (green) solid line at $x = 0$ indicates the interface plane. The inset shows the interface slab for DFT calculations in top view. White, black, and gray filled circles represent As, Ga, and Fe atoms, respectively.

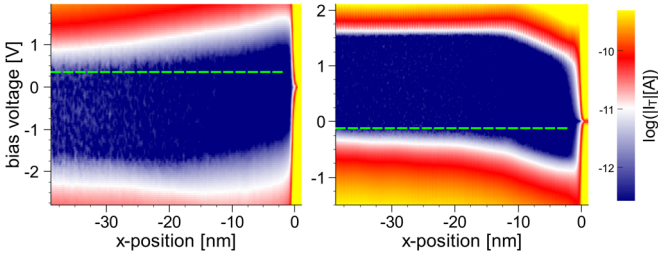

FIG. 2 (color online). 250 topography-normalized (see text) I-V spectra taken along the space charge region of (left) an n-type and (right) a p-type Fe/GaAs(110) interface. The tunnel current is plotted color coded as $\log(|I_T|)$ in dependence of bias voltage between tip and sample and x position (interface at $x = 0$ nm). Each I-V curve is averaged over three spectra in the y direction. Data (p type) taken at $T = 6$ K and (n type) at room temperature (RT). The horizontal green dashed lines serve as a guide to the eye for the flat band condition.

We prepare and measure our samples *in situ* without breaking the ultrahigh vacuum at any time. After a first cleavage along the GaAs(110) surface a 7 monolayer (ML) thick Fe film is epitaxially grown in a two-step low temperature growth process [29]. A perpendicular second cleavage gives access to the Fe/GaAs(110) interface [30]. Figure 1 shows a constant current topography of an Fe/n-GaAs(110) interface. The atomic corrugation of the Ga sublattice for a positive sample bias voltage V_s is clearly visible and continues up to the interface plane (solid green line). Figure 1 exhibits Fe protrusions of up to 1.5 Å in the z direction (elevations to the right of the interface) arising due to the ductility of the Fe film during the 2nd cleavage process at room temperature (RT). For our analysis we focus on regions where the Fe film and GaAs cleave virtually at constant apparent height in the z direction; e.g., see the region at the red dashed line ($y = y_0$) in Fig. 1. This selection is independent of the chosen bias voltage [30]. These regions allow direct access to the atomically flat interface with the STM tip and are the only ones considered throughout this Letter. There we do not find any signs of compound formation or intermixing. Hence, we conclude that the two-step growth process yields ideal and abrupt interfaces. This is also predicted by first-principles calculations where Grünebohm *et al.* [37] propose that a flat Fe/GaAs(110) interface becomes stable when the GaAs(110) surface is covered by a laterally closed Fe film of at least 1 ML thickness.

In order to investigate the electronic structure of the space charge region (SCR), we perform atomically resolved STS measurements by opening the feedback loop at each measurement point (x, y) and taking a current voltage (I-V) spectrum. We choose the voltage range and spatial range in such a way to obtain the course of the valence and conduction band for the entire SCR. In Fig. 2 we show cross-sectional STS spectra of (left) an n- and (right) a p-type doped interface, respectively. In total we take 250 I-V curves along the x direction perpendicular to the interface; see the Supplemental Material for spectral resolution [30]. The I-V spectra are topography normalized to a constant tip-sample distance which is of essential importance if one extracts quantitative information from the data as done later in this Letter [30]. The apparent band gap larger than the bulk value of 1.42 eV at RT and 1.52 eV at 6 K [38] is attributed to tip-induced band bending (TIBB) [39,40]. The energetic position of the band edges relative to the Fermi energy E_F depends on the x position. Towards the interface the conduction and valence bands clearly exhibit an upward and downward bending for n-type and p-type Fe/GaAs(110) interfaces, respectively. From Fig. 2 we obtain approximate SCR widths for the n-doped and p-doped sample of $w^n_{\mathrm{SCR}} \approx 40$ and $w^p_{\mathrm{SCR}} \approx 27$ nm, respectively, by finding the x position where valence and conduction bands flatten out indicated by the horizontal green dashed lines. If we assume SB heights of $\Phi^n_{\mathrm{SB}} = 0.8$ eV and $\Phi^p_{\mathrm{SB}} = 0.6$ eV as found in the literature [41,42] and take the donor (Si atoms) and acceptor (Zn atoms) concentrations of $N_D = 0.8 \times 10^{18}$ and $N_A = 2.75 \times 10^{18}$ cm^{-3} as specified by the manufacturer and confirmed by RT Hall measurements, we expect $w^n_{\mathrm{SCR}} \approx 38$ and $w^p_{\mathrm{SCR}} \approx 19$ nm, which is in reasonable agreement with our measurements.

For a realistic and quantitative investigation of the electronic properties of the ideal Fe/GaAs(110) interface based on local I-V spectra we have to take the three-dimensional (3D) superposition of SCR and TIBB into consideration. For this we present a 3D finite element method (FEM) approach that includes the detailed 3D geometry and electrostatic features of our experiment. By solving the Poisson equation for n-type (p-type) contacts, the 3D FEM calculations yield the vacuum tunneling (VT) energy range Φ_{VT} between the conduction band minimum E_C (valence band maximum E_V) and the Fermi level of the tip E^M_F for positive (negative) sample bias voltages [Fig. 3(a)]. Within the energy range Φ_{VT} electrons tunnel solely through the vacuum barrier between tip and sample. Only in the energy range Φ_{VT} a significant tunnel current I_T exists [30,39]. Therefore, Φ_{VT} can be thought of as a

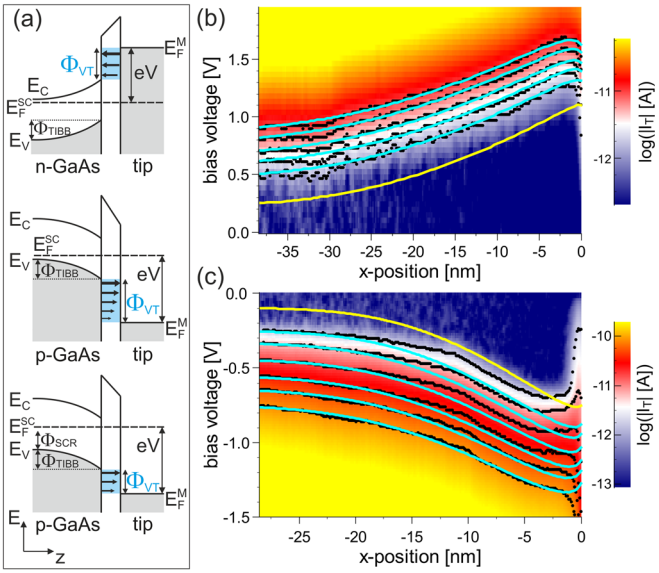

FIG. 3 (color online). (a) Scheme of the vacuum tunneling (VT) energy range Φ_{VT} in the rigid band model. For more details see text. (b) and (c) The tunnel current is depicted color coded as $\log(|I_T|)$ for 250 topography-normalized I-V spectra along the x axis across (b) an n-type and (c) a p-type interface (interface at $x = 0$ nm). Data taken at (b) RT and (c) $T = 6$ K. The black dots represent isolines of constant current. The light blue solid lines represent isolines from 3D finite element calculations (see text). Yellow isolines represent the band edges in the rigid band model.

measure for I_T, and thus allows a comparison between experiment and simulation; see Ref. [30] for details on our approach.

Figure 3(b) shows topography-normalized spectra perpendicular to an n-type Fe/GaAs(110) interface for positive voltages. The black dots represent isolines of constant tunnel current I_T. The colored solid lines depict isolines of constant Φ_{VT} simulated for a SB height of $\Phi^n_{SB} = 0.94(3)$ eV. For this SB height the Φ_{VT} isoline and the experimental I_T isoline deepest inside the conduction band (starting at $V_s = 0.9$ V) exhibit the smallest deviation from each other. Deep inside the conduction band we expect the smallest disturbance of the tunnel current due to charged dopant atoms in proximity. For more details on SB height extraction see Ref. [30]. The MIGS-and-electronegativity model predicts $\Phi^n_{SB} = 0.96$ eV [43], which is in excellent agreement with our experimental data. Figure 3(b) clearly shows that the 3D FEM simulation, where we consider only electrostatic effects (band bending of the SCR and TIBB), excellently describes the experimental data of the conduction band along the SCR. However, energetically lower lying I_T isolines exhibit deviations from the electrostatic rigid band model isolines at about 2 nm off the interface. The yellow isoline represents the conduction band edge one would expect in the electrostatic rigid band model. Evidently, there is some additional tunnel current inside the band gap at the interface.

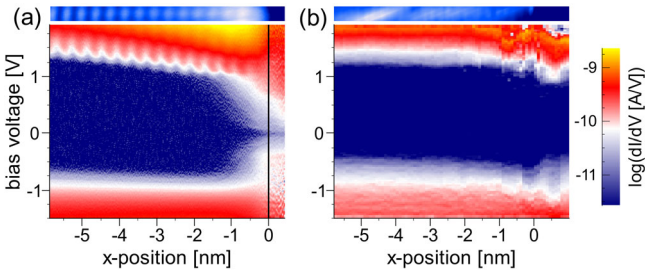

FIG. 4 (color online). Color-coded dI/dV spectra calculated from (a) 230 respective I-V spectra taken across a p-type interface along the atomic line in the x direction depicted above ($V_s = +1.75$ V, $I_T = 75$ pA) and (b) from 100 respective I-V spectra taken across a p-type GaAs(110)-(1$\bar{1}$0) edge. The data are averaged over 10 spectra in the y direction. The interface and the edge are both located at $x = 0$ nm.

In Fig. 3(c) the data for a p-type junction are plotted. The best fit deep inside the valence band we find for a SB height of $\Phi^p_{SB} = 0.78(2)$ eV. The MIGS-and-electronegativity model predicts a much smaller SB height of $\Phi^p_{SB} = 0.46$ eV [43] at RT and cannot explain our experimental value. Again we observe a pronounced tunnel current inside the band gap at the interface.

To further investigate the microscopic origin of the Fermi level pinning mechanism, we have analyzed the immediate interface region on the atomic scale. Figure 4(a) shows atomically resolved STS data taken across a p-doped Fe/GaAs(110) interface. We calculate the differential conductance from respective I-V spectra as a direct measure for the LDOS. For positive bias voltages the surface resonances C_3 and C_4 localized on surface cations [28] are addressed revealing the Ga sites as maxima at the conduction band edge. In contrast to the clearly visible atomic corrugation in the conduction band, the I-V spectra show a spatial and energetic continuum of states in the band gap in the first few GaAs layers at the interface. Most notably, there are no signs of localized states inside the band gap neither in energy nor in real space. Thus, we do not find any evidence of defect-induced gap states which further corroborates a defect-free interface. The observed gap states are found along the entire interface and are virtually not affected by local variations of Fe film protrusions or vacancies at the interface [30]. At the band edges the gap states extend 3–4 unit cells into the band gap. Exponential fits at midgap yield the smallest decay length of $\lambda \approx 4$ Å. This is in good agreement with other experimental findings of $\lambda \approx 3.4$ Å measured at Fe clusters on GaAs(110) [21]. Calculations considering the complex band structure of GaAs yield a midgap decay length of $\lambda \approx 3$ Å [7]. A control experiment across a p-type GaAs(110)-(1$\bar{1}$0) edge without Fe film does not exhibit any gap states [Fig. 4(b)]. This demonstrates that dangling bonds or the abrupt potential change at the immediate edge do not produce surface states inside the band gap. Therefore, our experiment reveals a purely interface-induced

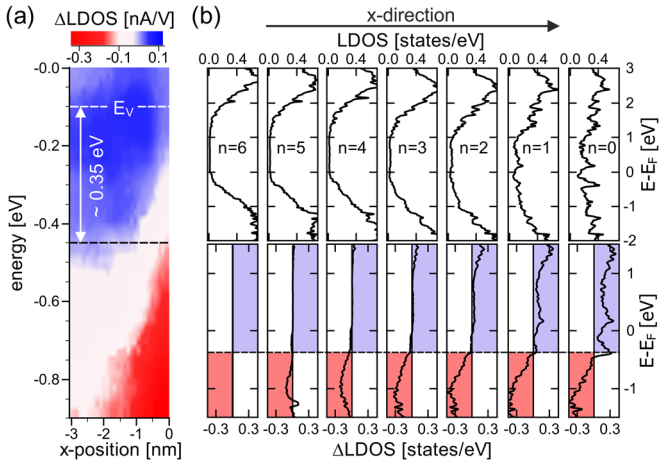

FIG. 5 (color online). (a) Variation of the LDOS inside the valence band for a p-type junction extracted from the STS data set in Fig. 3(c) (interface at $x = 0$ nm). The white dashed line represents the valence band edge E_V. (b) Density functional calculations for the ideal Fe/GaAs(110) interface: (upper panels) The total (sum of spin-up and -down) density of states of the nth GaAs layer off the interface. The Fermi energy is located at the valence band edge. (lower panels) Variation of the LDOS in the nth GaAs layer with respect to the 6th layer. At 0.35 eV below the valence band edge (horizontal dashed line) we observe a sharp drop in ΔLDOS (transparent red area) due to Fe-As hybridization (see text).

continuum of gap states for ideal Fe/GaAs(110) interfaces. Furthermore, the long-range STS data in Fig. 3(c) nicely shows the diverging character of these gap states at the band edge. All this is in striking analogy to the MIGS model.

Moreover, for the p-type interface in Fig. 3(c) we observe strong deviations between measurement and simulation inside the valence band. The experimental I-V data consist of an electrostatic part (band bending along the SCR and TIBB) and an interface specific part due to charge rearrangement at the interface. Using the 3D FEM data we remove the electrostatic part from the I-V data by reading out the tunnel current data along the simulated rigid band Φ_{VT} isolines. Subsequently, we differentiate this data along the energy axis and subtract the offset far away from the interface. This yields the spatial and energetic variation of the local density of states ΔLDOS with respect to the free surface [see Fig. 5(a)]. One distinctive feature is the increase of ΔLDOS close to the valence band edge. More strikingly, at the interface we find a rather localized decrease in ΔLDOS about 0.35 eV below the valence band edge.

For a deeper understanding we perform density functional theory (DFT) calculations. We have chosen a slab of 9 layers of GaAs and 2 layers of Fe [inset Fig. 1]; for more details see Ref. [30]. Within the DFT calculations periodic boundary conditions are applied whereas the experimental setup has a broken symmetry along the z direction [see Fig. 1]. As shown in the upper panels in Fig. 5(b), the DFT calculations show a continuum of states inside the band gap within the first 3–4 layers at the interface. Furthermore, the asymmetric behavior of the decay lengths of the gap states, with slightly larger lengths on the conduction band side, is in good agreement with the experimental data [Fig. 4(a)]. Moreover, the DFT calculations yield a SB height of $\Phi_{SB}^{p} = 0.69$ eV which is much closer to our experimental value and in stark contrast to the MIGS-and-electronegativity model. We obtain ΔLDOS from the DFT data by subtracting the LDOS of our reference "bulk" layer ($n = 6$) from the LDOS of the nth layer, cf. lower panels in Fig. 5(b). At the interface the DFT data show a sharp decrease of the LDOS with respect to the bulk at 0.35 eV below the valence band edge as observed in the experimental data. Since our cross-sectional STS approach yields an LDOS variation map that is stunningly similar to DFT predictions [see Fig. 5], we reason that our experimental technique can serve as an excellent probe to study the microscopic origin of the MS interface dipole.

By analyzing the DFT data of the LDOS at individual atomic sites [30] we find a strong hybridization between the majority states of Fe and As inside the valence band. Thus, a detailed atomic description of the interface in the sense of the bond polarization model is necessary to explain our experimental p-type SB height and the variation of the LDOS inside the valence band. The experimentally observed p-type SB height requires a modification of the interface dipole with respect to the pure MIGS model and can be qualitatively explained by the additional positive charge inside the valence band due to Fe-As hybridization, which partially compensates the negative charge of the MIGS. Experimentally, the downward shift of the valence band edge with respect to the Fermi energy is ∼0.3 eV larger for the p-type than for the n-type interface. This relative energetic shift between the GaAs and Fe band structures seems to increase the impact of bond polarization significantly.

In conclusion, providing the electronic properties at an ideal Fe/GaAs(110) interface on the atomic scale our experiment serves as a reference for future studies on the influence of defects and the detailed atomic structure at the interface on SB formation. By means of scanning tunneling spectroscopy we measure the LDOS at the interface on a broad energy range with atomic resolution exploring the relevance of MIGS and bond polarization models. High resolution data show a continuum of interface-induced gap states. Furthermore, for p-type samples we find an LDOS modification in the valence band at the interface and a SB height that strongly deviates from the MIGS model prediction. DFT calculations show both MIGS and bond polarization at the interface and are in excellent agreement with the experimental findings.

Support by the Deutsche Forschungsgemeinschaft through priority program SPP 1285 is gratefully acknowledged.

*mwender@gwdg.de

[1] W. Schottky, Phys. Z. **41**, 570 (1940).
[2] N. F. Mott, Proc. Cambridge Philos. Soc. **34**, 568 (1938).
[3] R. T. Tung, Mater. Sci. Eng. R **35**, 1 (2001).
[4] W. Mönch, *Semiconductor surfaces and interfaces*, edited by G. Ertl, R. Gomer, H. Lüth, and D. L. Mills (Springer, Berlin, Heidelberg, Germany, 2001).
[5] V. Heine, Phys. Rev. **138**, A1689 (1965).
[6] S. G. Louie, J. R. Chelikowsky, and M. L. Cohen, Phys. Rev. B **15**, 2154 (1977).
[7] J. Tersoff, Phys. Rev. Lett. **52**, 465 (1984).
[8] W. Mönch, Phys. Rev. Lett. **58**, 1260 (1987).
[9] W. E. Spicer, Z. Lilienthal-Weber, E. Weber, N. Newman, T. Kendelewicz, R. Cao, C. McCants, P. Mahowald, K. Miyano, and I. Lindau, J. Vac. Sci. Technol. B **6**, 1245 (1988).
[10] R. T. Tung, Phys. Rev. Lett. **84**, 6078 (2000).
[11] R. T. Tung, Phys. Rev. B **64**, 205310 (2001).
[12] R. T. Tung, J. M. Gibson, and J. M. Poate, Phys. Rev. Lett. **50**, 429 (1983).
[13] R. T. Tung, Phys. Rev. Lett. **52**, 461 (1984).
[14] D. R. Heslinga, H. H. Weitering, D. P. van der Werf, T. M. Klapwijk, and T. Hibma, Phys. Rev. Lett. **64**, 1589 (1990).
[15] K. Yamane, K. Hamaya, Y. Ando, Y. Enomoto, K. Yamamoto, T. Sadoh, and M. Miyao, Appl. Phys. Lett. **96**, 162104 (2010).
[16] K. Kasahara, S. Yamada, K. Sawano, M. Miyao, and K. Hamaya, Phys. Rev. B **84**, 205301 (2011).
[17] W. J. Kaiser and L. D. Bell, Phys. Rev. Lett. **60**, 1406 (1988).
[18] A. A. Talin, R. S. Williams, B. A. Morgan, K. M. Ring, and K. L. Kavanagh, Phys. Rev. B **49**, 16474 (1994).
[19] H.-J. Im, Y. Ding, J. P. Pelz, and W. J. Choyke, Phys. Rev. B **64**, 075310 (2001).
[20] R. M. Feenstra and P. Mårtensson, Phys. Rev. Lett. **61**, 447 (1988).
[21] P. N. First, J. A. Stroscio, R. A. Dragoset, D. T. Pierce, and R. J. Celotta, Phys. Rev. Lett. **63**, 1416 (1989).
[22] R. M. Feenstra, Phys. Rev. Lett. **63**, 1412 (1989).
[23] R. M. Feenstra, J. Vac. Sci. Technol. B **7**, 925 (1989).
[24] T. C. G. Reusch, M. Wenderoth, L. Winking, N. Quaas, and R. G. Ulbrich, Phys. Rev. Lett. **93**, 206801 (2004).
[25] T. C. G. Reusch, M. Wenderoth, L. Winking, N. Quaas, and R. G. Ulbrich, Appl. Phys. Lett. **87**, 093103 (2005).
[26] G. A. Prinz and J. J. Krebs, Appl. Phys. Lett. **39**, 397 (1981).
[27] T. W. Kim and Y. S. Yoon, J. Phys. Chem. Solids **61**, 847 (2000).
[28] J. R. Chelikowsky and M. L. Cohen, Phys. Rev. B **20**, 4150 (1979).
[29] L. Winking, M. Wenderoth, J. Homoth, S. Siewers, and R. G. Ulbrich, Appl. Phys. Lett. **92**, 193102 (2008).
[30] See Supplemental Material at http://link.aps.org/supplemental/10.1103/PhysRevLett.114.146804, which includes Refs. [31–36], for details on the low temperature preparation process, on the bias dependence of the apparent height at the interface, on the spectral resolution, on the projection of the STS data by topography normalization, for a detailed description of our 3D finite element method approach, for details on the extraction of the Schottky barrier height from the data, for a discussion of the interface states, and for more details on the density functional calculation.
[31] E. F. Schubert, *Doping in III-V semiconductors* (Cambridge University Press, Cambridge, England, 1993).
[32] G. Münnich, A. Donarini, M. Wenderoth, and J. Repp, Phys. Rev. Lett. **111**, 216802 (2013).
[33] K. Teichmann, Ph.D. thesis, Georg-August-University, Göttingen, 2012.
[34] The Jülich full-linearized augmented plane waves (FLAPW) code family: http://www.flapw.de.
[35] J. P. Perdew, K. Burke, and M. Ernzerhof, Phys. Rev. Lett. **77**, 3865 (1996).
[36] I. V. Solovyev, P. H. Dederichs, and V. I. Anisimov, Phys. Rev. B **50**, 16861 (1994).
[37] A. Grünebohm, H. C. Herper, and P. Entel, Phys. Rev. B **80**, 064417 (2009).
[38] S. M. Sze, *Physics of semiconductor devices, second edition* (John Wiley & Sons, New York, 1981).
[39] R. M. Feenstra and J. A. Stroscio, J. Vac. Sci. Technol. B **5**, 923 (1987).
[40] R. M. Feenstra, J. Vac. Sci. Technol. B **21**, 2080 (2003).
[41] G. Myburg, F. D. Auret, W. E. Meyer, C. W. Louw, and M. J. Staden, Thin Solid Films **325**, 181 (1998).
[42] J. R. Waldrop, Appl. Phys. Lett. **44**, 1002 (1984).
[43] W. Mönch, *Electronic properties of semiconductor interfaces*, edited by G. Ertl, H. Lüth, and D. L. Mills (Springer, Berlin, Heidelberg, Germany, 2004).